Gene 960 (2025) 149539

Contents lists available at ScienceDirect

Gene

journal homepage: www.elsevier.com/locate/gene

Lrig3-deficient mice exhibit strain-specific alterations in liver fat accumulation, intestinal morphology, and middle ear inflammation

Carl Herdenberg [a], Roger Henriksson [a], Håkan Hedman [a,*], Veronica Rondahl [b,c]

[a] Department of Diagnostics and Intervention, Oncology, Umeå University, SE-90187 Umeå, Sweden
[b] Department of Pathology and Wildlife Disease, National Veterinary Institute (SVA), SE-751 89 Uppsala, Sweden
[c] Department of Animal Biosciences, Division for Anatomy, Physiology, Immunology, and Pathology, Swedish University of Agricultural Sciences, SE-750 07 Uppsala, Sweden[1]

A B S T R A C T

The transmembrane protein leucine-rich repeats and immunoglobulin-like domains 3 (LRIG3) regulates fat metabolism and bone morphogenetic protein (BMP) signaling. *Lrig3*-deficient mice exhibit impaired development of the snout and the inner ear lateral canal, neural defects, and cardiac hypertrophy in adulthood. However, no thorough and unbiased analysis of the physiological functions of *Lrig3* has previously been performed. To address this knowledge gap, we performed histopathological examination of 42 tissues and organs from 1-year-old female C57BL/6JBomTac and 129S1-U mice with different *Lrig3* genotypes. Among the scored pathologies, three were significantly associated with *Lrig3* genotype: spontaneous macrovesicular hepatocellular degeneration (hepatocellular steatosis) was less prevalent in *Lrig3*-deficient C57BL/6JBomTac mice, whereas dilated or flaccid ileum and otitis media were more common in *Lrig3*-deficient 129S1-U mice. To further investigate hepatic steatosis phenotypes, 8-week-old C57BL/6JBomTac mice of both sexes and different *Lrig3* genotypes were subjected to consuming a high-fat diet (HFD) for 8 weeks. The HFD regimen led to relatively few cases of hepatocellular steatosis, with no significant differences among the genotypes; however, female *Lrig3*-deficient mice presented reduced microvesicular hepatocellular degeneration compared with their wild-type littermates. This study revealed that *Lrig3* regulates liver fat accumulation, intestinal morphology, and middle ear inflammation in a mouse strain-dependent manner.

1. Introduction

The leucine-rich repeats and immunoglobulin-like domains (LRIG) protein family consists of three structurally similar transmembrane proteins; LRIG1 (Suzuki et al., 1996; Nilsson et al., 2001), LRIG2 (Holmlund et al., 2004), and LRIG3 (Guo et al., 2004). LRIG1, the most studied family member, has been implicated in many different biological functions, such as tumor suppression (Powell et al., 2012; Wang et al., 2013; Neirinckx et al., 2017), the regulation of growth factor signaling (Gur et al., 2004; Laederich et al., 2004; Simion et al., 2014; Lindquist et al., 2014), and the regulation of stem cell quiescence (Jensen et al., 2009; Powell et al., 2012; Wong et al., 2012; Herdenberg and Hedman, 2023). Additionally, we recently showed that LRIG1 and LRIG3 regulate fat metabolism by promoting bone morphogenetic protein (BMP) signaling (Herdenberg et al., 2021). LRIG3 is less studied than LRIG1. LRIG3 reportedly has similar or opposing functions as LRIG1 (Del Rio et al., 2013; Rafidi et al., 2013; De Vincenti et al., 2021), and the two proteins may also physically and functionally interact with one another (Faraz et al., 2018). The BMP signal-regulating functions of LRIG1 and LRIG3 are redundant or distinct depending on the specific BMP ligands involved (Herdenberg et al., 2021; Abdullah et al., 2023). In humans, certain *LRIG3* gene variants are associated with skeletal proportions, i.e., hip width (Kun et al., 2023), plasma levels of high-density lipoprotein (HDL) cholesterol (Ma et al., 2010; Manichaikul et al., 2022), and the risk of incident heart failure (Smith et al., 2010). In domestic animals, single-nucleotide polymorphisms (SNPs) in or near the *LRIG3* sequence have been associated with pig litter size (Metodiev et al., 2018), pig birth weight (Óvilo et al., 2022), lamb birth weight (Abousoliman et al., 2021), selection of Charolais beef cattle (Xu et al., 2015), selection of Greyhound racing dogs (Akey et al., 2010), and selection of Luxi

Abbreviations: LRIG, Leucine-rich Repeats and Immunoglobulin-like Domains (human); Lrig, Leucine-rich Repeats and Immunoglobulin-like Domains (mouse); BMP, Bone Morphogenetic Protein; HFD, High-Fat Diet; HDL, High-Density Lipoprotein; SNP, Single-Nucleotide Polymorphism; IMPC, International Mouse Phenotyping Consortium; PCR, polymerase chain reaction; ddPCR, droplet digital PCR; ENA, European Nucleotide Archive; VCF, Variant Call Format; LD, Linkage Disequilibrium; NGI, National Genomics Infrastructure; NAISS, National Academic Infrastructure for Supercomputing in Sweden; NBIS, National Bioinformatics Infrastructure Sweden; ko, knockout; wt, wild type; hz, heterozygote.

* Corresponding author at: Oncology Research Laboratory, NUS M31, SE-90185 Umeå, Sweden.
E-mail address: hakan.hedman@umu.se (H. Hedman).

[1] Current affiliation.

https://doi.org/10.1016/j.gene.2025.149539
Received 29 January 2025; Received in revised form 13 April 2025; Accepted 30 April 2025
Available online 2 May 2025

gamecocks (Zhou et al., 2023).

Lrig3-deficient mice are viable (Abraira et al., 2008). However, to date, studies regarding *Lrig3*-deficient mice have been limited to substrains of C57BL/6 or mice of mixed genetic backgrounds, and they have focused on specific traits. Goodrich and coworkers, using the C57BL/6J substrain, reported that *Lrig3*-deficient mice presented with a shortened snout and a defect in inner ear development (Abraira et al., 2008; Del Rio et al., 2013). Hedman and coworkers, also using the C57BL/6J substrain, reported that *Lrig3*-deficient female mice presented with cardiac hypertrophy and altered HDL cholesterol levels (Hellström et al., 2016). Paratcha and coworkers, using mice of mixed genetic backgrounds, reported that *Lrig3* deficiency combined with *Lrig1* heterozygosity resulted in increased epidermal innervation of cold-sensitive nonpeptidergic nociceptive neurons (De Vincenti et al., 2021). Additionally, the International Mouse Phenotyping Consortium (IMPC) has performed general phenotyping of a limited number of *Lrig3*-deficient C57BL/6N mice and has confirmed the cardiac (Hellström et al., 2016) and skull (Abraira et al., 2008) phenotypes and revealed additional abnormalities in the skeleton, skeletal muscles, thymus, kidneys, and spleen, as well as male and female infertility (https://www.mousephenotype.org; Dickinson et al., 2016; Groza et al., 2023). To our knowledge, no thorough histopathological examination of *Lrig3*-deficient mice with any genetic background has been presented, nor has a comparison between the *Lrig3* knockout phenotypes of different mouse strains been previously performed. We are also not aware of any investigations addressing the incidence of tumors in *Lrig3*-deficient mice.

Here, we performed a histopathological examination of 42 different organs and tissues from 1-year-old wild-type, *Lrig3*-heterozygous, and *Lrig3*-knockout female mice on the C57BL/6JBomTac and 129S1-U genetic backgrounds. We describe both strain-dependent and strain-independent *Lrig3*-knockout phenotypes. Strikingly, *Lrig3*-deficient C57BL/6JBomTac mice presented with a reduced incidence of spontaneous fatty liver, whereas *Lrig3*-deficient 129S1-U mice presented with a dilated or flaccid ileum and an increased incidence of otitis media. We also performed a high-fat diet (HFD) experiment and showed that *Lrig3*-deficient female C57BL/6JBomTac mice developed fewer microvesicles in their livers under this dietary regimen.

2. Materials and methods

2.1. Ethics statement and animal husbandry

All the mice were housed and maintained in accordance with European Communities Council Directive (86/609/EEC). The experimental protocols were approved by the Regional Ethics Committee of Umeå University, Umeå, Sweden (registration nos. A193–12 and A31–2017). The animals were housed under controlled conditions with a 12-h day/night cycle and provided water and either standard chow pellets (cat. no. 801730, Special Diets Services, NOVA-SCB Sweden, Sollentuna, Sweden) or a HFD consisting of 60 % fat (D12492, Research Diets, Inc., New Brunswick, NJ, USA) ad libitum. In the 1-year experiment, 70 female C57BL/6JBomTac mice and 72 female 129S1-U mice were analyzed. Two C57BL/6JBomTac mice were excluded after analysis because of discrepancies in their identification numbers. In total, 24 *Lrig3*+/+, 20 *Lrig3*+/-, and 24 *Lrig3*-/- C57BL/6JBomTac mice, and 22 *Lrig3*+/+, 24 *Lrig3*-/-, and 26 *Lrig3*-/- 129S1-U mice were included in the analyses. In the HFD experiment, 70 C57BL/6JBomTac mice were analyzed, and one was excluded due to a discrepancy in genotyping. The investigator was blinded to the specific genotypes of the mice. The mouse colony was routinely screened and found to be negative for mouse hepatitis virus.

2.2. Lrig3 modifications and genotyping

The *Lrig3* allele $Lrig3^{tm1.1Hhed}$ lacks exon 1 of *Lrig3*, which includes the predicted ATG start codon (Hellström et al., 2016). $Lrig3^{tm1.1Hhed}$ was transferred to a pure mouse genetic background by backcrossing with the C57BL/6JBomTac and 129S1-U mouse strains for ten generations. Mice of different *Lrig3* genotypes were obtained through mating of mice that were heterozygous for the *Lrig3* mutant allele $Lrig3^{tm1.1Hhed}$. Homozygous B6.129-$Lrig3^{tm1.1Hhed}$ mice have been confirmed to lack measurable levels of the full-length *Lrig3* protein by Western blotting (Hellström et al., 2016). Genotyping of the *Lrig3* allele was performed twice for each animal; at weaning using conventional polymerase chain reaction (PCR) protocols for the floxed wild-type allele or the knockout allele and again to confirm the genotype at the end of the experiment using DNA prepared from the liver and a previously described duplex droplet digital PCR (ddPCR) assay (Herdenberg et al., 2021). The PCR primer and probe sequences are shown in Supplementary Table 1.

2.3. Mouse strain identities

C57BL/6JBomTac mice were obtained from Taconic Biosciences (Ejby, Denmark), and 129S1 strain mice were obtained from local colleagues. Prior to this study, the two mouse strains were maintained at our animal facility for an unknown number of generations. Mouse strain identities were validated through whole-genome sequencing via the SNP&SEQ technology platform (SciLifeLab, Uppsala, Sweden). The sequences were deposited at the European Nucleotide Archive (ENA): PRJEB82724. The sequence analysis was based on the sarek nf-core pipeline. Sarek (version 3.4.2) was run, providing the four Illumina sequencing samples, the GRCm39 mouse reference assembly and the use of freebayes as variant callers and default parameters otherwise. The resulting variant call format (VCF) files were merged with a reference VCF file, which represents a complete SNP variation catalog of 52 inbred mouse strains (PRJEB53906), using BCFtools merge (version 1.20). The merged VCF file was further filtered for high-quality SNPs by using BCFtools view and the following filter criteria: minimum quality >=30, minimum coverage depth >=15 and variant type = snps. Plink2 (version: 2.00 Alpha 5.14) was used to calculate the linkage disequilibrium (LD) with a window size of 10 kb, thresholds of 0.5 and 0.2 and the omission of sex chromosomes and mitochondria (X, Y and NC_005089.1). The resulting pruned SNP subset, which consists of the variants that are in approximate linkage equilibrium, represents the final VCF file. This file was converted into a sequence alignment format (PHYLIP) with the python script vcf2phylip (version 2.8) and different thresholds for the minimum samples argument, which defines the minimum number of samples to be present at each SNP locus (n = 36,41,46,51,56). The SPRET-EiJ strain was used as an outgroup. The resulting alignment files were then used to create phylogenetic trees with IQTREE software (version 2.3.6) by using a bootstrap size of 1000 replicates −B 1000 and the recommended model GTR + ASC for SNP data, which accounts for an ascertainment bias correction. FigTree (version 1.4.4) was used to visualize the resulting phylogenetic tree models. To obtain a more precise estimate of the exact C57BL/6 substrain of samples #6784 and #7161, a genetic analysis was performed, which was based on the findings of Mekada and Yoshiki (Mekada and Yoshiki, 2021). They analyzed 45 selected SNP markers for multiple C57BL/6J and C57BL/6N substrains, including C57BL/6J, C57BL/6JJcl, C57BL/6JJmsSlc, C57BL/6JBomTac, C57BL/6JOlaHsd, C57BL/6JRccHsd, C57BL/6JRj, C57BL/6JMs, C57BL/6JNrs, C57BL/6NJ, C57BL/6NCrl, C57BL/6NCrlCrlj, C57BL/6NJcl, C57BL/6NCrSlc, C57BL/6NSea, C57BL/6NTac, C57BL/6NHsd, C57BL/6NRj, C57BL/6NHla, C57BL/6NCrSim, and C57BL/6ByJ. On the basis of the read alignments and variant calls of samples #6784 and #7161, all 45 marker SNPs were manually inspected with the IGV browser.

2.4. Glucose measurements

For the HFD experiment, blood glucose levels were measured every other week. The mice were fasted for six hours before whole blood was collected from the facial veins. Glucose levels were analyzed within two

hours after blood sampling using a Contour XT blood glucose meter (Acensia Diabetes Care, Basel, Switzerland).

2.5. Blood chemical analyses

The chemical compositions of whole blood sampled from the facial veins, were analyzed after 6 hours of fasting. A Vetscan VS2 Chemistry analyzer (Abaxis Triolab, Mölndal, Sweden) with a Vetscan preventive care profile plus rotors (Abaxis Triolab) was used according to the manufacturer's instructions. For insulin measurements, the blood was centrifuged at 4 °C for 20 min at 2,000 × g, followed by collection of the plasma fraction, which was frozen at −80 °C until analysis. Insulin was analyzed using an ultrasensitive mouse insulin ELISA kit using a wide range assay (cat. no. 90080; Chrystal Chem, Zaandam, The Netherlands).

2.6. Echo-MRI

At the beginning and end of the HFD experiment, lean and fat tissues were measured using an Echo-MRI 100 system (Echo Medical Systems, Houston TX, USA) according to the manufacturer's instructions. The mice were weighed before the measurements.

2.7. Tissue preparation

At the end of the 1-year study and the HFD experiment, the mice were euthanized by CO_2 exposure and necropsied by specially trained staff. All the tissues, including the body, were collected and fixed in 4 % phosphate-buffered formalin. All the fixed materials were examined and trimmed by a veterinary anatomic pathologist with experience in laboratory animal pathology (VR) who was blinded to the specific genotypes of the sample. The organs and tissues that were included were the adrenal gland, brain, cecum, cervix, colon, duodenum, ear, esophagus, eye, gall bladder, harderian gland, heart, hind leg, ileum, jejunum, kidney, liver, lung hilus, lung lobes, lymph nodes (axillar, mediastinal, mesenteric, pancreatic, submandibular), ovary, oviduct, pancreas, rectum, salivary glands (parotid, sublingual, submandibular), skeletal muscle, skin, spleen, stomach, thymus, tissues of the skull, trachea, urinary bladder, uterus, and vagina (Supplementary Table 1). The trimmed material was paraffin-embedded, cut into 4-µm sections, and stained with Mayer's hematoxylin and eosin according to standard protocol.

2.8. Pathological evaluation

The tissue samples were analyzed and scored by a veterinary anatomic pathologist experienced in laboratory animal pathology (VR) who was blinded to the specific genotypes of the samples. The scoring was semiquantitative and performed as described by Mann et al. (Mann et al., 2012). In brief, tissue with an appearance within normal limits, considering the age, sex, and strain of the mice, was given a score of 0. Lesions with minimal change, i.e., the amount of change barely exceeded change that was considered to be within normal limits, were given a score of 1. Lesions with mild change, i.e., the lesion was easily identified but of limited severity, were given a score of 2. Lesions with moderate change, i.e., the lesion was prominent but there was significant potential for increased severity, were given a score of 3. Lesions with severe change, i.e., the degree of change occupied the majority of the organ, were given a score of 4. For some lesions, e.g., cysts or neoplasias, a binomial score was used – yes if a lesion was present and no if a lesion was absent (Supplementary Table 1).

2.9. Statistical analyses

Two-sided t tests were used to assess statistical patterns between groups with numerical dependent variables. For categorical dependent variables, the Kruskal–Wallis test and logistic regression were used. Only morphological characteristics that were scored as present in at least 10 % of the mice were included. Statistical analysis was performed using Prism 8 or R-studio (version 1.1463) using R (version 3.5.3). In all the statistical analyses, except in the initial phenotype screen, p values < 0.05 were considered significant. To account for multiple testing in the initial phenotype screen, p values < 0.01 were considered significant in this analysis.

3. Results

3.1. Mouse strain verification

The current study was performed using inbred mice of two different genetic backgrounds, one C57BL/6 strain and one 129S1 strain, both of which were maintained by in-house breeding at our animal facility. To verify the mouse substrain identities, we performed whole-genome sequencing on two mice of each strain (mice #6784/7161 and #7123/7278), and conducted a phylogenetic analysis against 52 known laboratory mouse strains, with the strain SPRET-EiJ used as the outgroup. We tested different strictness values for the LD calculation (0.5 vs. 0.2) as well as different minimum numbers of samples to be present at each locus (n={36,41,46,51,56}). In total, this yielded 200 different phylogenetic trees, all revealing a nearly identical structure, in which mice #6784 and #7161 were always grouped into the C57BL* strain cluster and mice #7123 and #7278 were always grouped into the 129* strain cluster (Fig. 1). Mice #7123 and #7278 were most similar to strain 129S1-SvlmJ and were therefore designated 129S1-U. Mice #6784 and #7161 were most similar to strain C57BL-6NJ. To obtain a more precise estimate regarding the C57BL/6 substrains of samples #6784 and #7161, a genetic analysis comprising 45 diagnostic SNPs was performed. Both samples were in full agreement with the 44 marker SNPs that are present in the C57BL/6JBomTac substrain. Only the dBSNP ID *rs13459122* (chromosome 10 at 80,795,365 bp) was discordant with this conclusion. *rs13459122* has a T/T allele in C57BL/6JBomTac but had an A/A allele in samples #6784 and #7161. However, the GRCm38.p6 reference assembly had an A at position 80,795,365 (see the UCSC Genome Browser), which was apparently incorrectly listed in (Mekada and Yoshiki, 2021). Therefore, we excluded *rs13459122* from this analysis. Thus, in summary, all 44 conclusive marker SNPs in both #6784 and #7161 matched the substrain C57BL/6JBomTac. Hence, our 129S1 mouse strain was designated 129S1-U, and our C57BL/6 mouse strain was designated C57BL/6JBomTac.

3.2. Analysis of one-year-old Lrig3-deficient C57BL/6BomTac and 129S1-U mice

To investigate the role of *Lrig3* in mouse development and physiology, we performed necropsies and histopathological examinations of 1-year-old female C57BL/6JBomTac and 129S1-U mice with different *Lrig3* genotypes. Female mice were chosen on the basis of a previous study in which *Lrig3*-deficient female C57BL/6JBomTac mice tended to have an increased incidence of abdominal neoplasia (Hellström et al., 2016). We included two different mouse strains to discriminate between the general and strain-specific roles of *Lrig3*. The mice were fed a regular chow diet under standard mouse husbandry conditions for one year, after which they were euthanized and necropsied. For each mouse, 42 different tissues and organs were examined and scored with regard to over 200 different histopathological features. Of these histopathological features, 154 were scored as aberrant in at least one animal (Supplementary Table 2). Two *Lrig3* -/- C57BL/6JBomTac mice died before one year of age. They were too decomposed to be necropsied and were therefore excluded from the study.

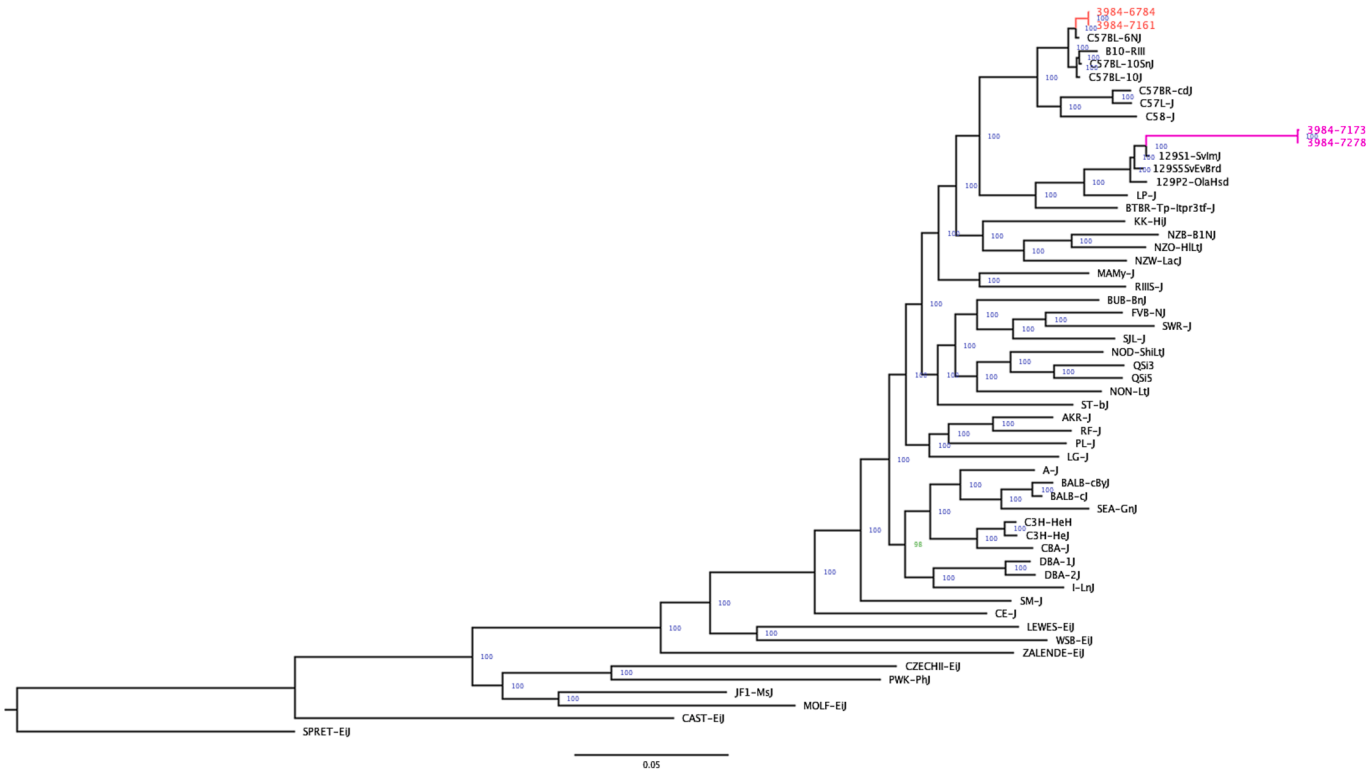

Fig. 1. Phylogenetic tree of 52 mouse strains and four samples from the current study. The samples grouped together are colored red (#6784 and #7161) and magenta (#7123 and #7278). Bootstrap values are labeled in blue and green and are represented in percentages [98,100]. The model was based on the full set of autosomes, LD (=0.5) and at least 41 samples for each of the 2,718,596 SNPs.

3.3. Lrig3-deficient female mice had reduced body weights at twelve months of age

In mice from both the C57BL/6JBomTac and 129S1-U backgrounds, the *Lrig3* genotype had an effect on body weight (Table 1, $p < 0.0001$ for each strain, Student's *t* test) (Fig. 2A). The *Lrig3-/-* mice had lower body weights than both the *Lrig3*+/+ mice (C57BL/6JBomTac $p < 0.0001$ and 129S1-U $p = 0.0013$, Tukey's multiple comparisons test) and the *Lrig3*+/- mice (C57BL/6JBomTac $p < 0.0001$ and 129S1-U $p = 0.0003$, Tukey's multiple comparisons test). The C57BL/6JBomTac *Lrig3-/-* mice had on average 21 % (7.5 g) lower body weights than *Lrig3*+/+ mice, and the 129S1-U *Lrig3-/-* mice had, on average, 11 % (2.9 g) lower body weights than *Lrig3*+/+ mice. A subset of mice was also scored for body condition; this analysis revealed a nonsignificant trend for C57BL/6JBomTac *Lrig3-/-* mice to have lower body condition scores than *Lrig3*+/+ mice did ($p = 0.04687$, Supplementary Table 2). There was no such trend observed in the 129S1-U mice ($p = 1.000$).

3.4. Lrig3-deficient C57BL/6JBomTac mice had a reduced incidence of hepatocellular macrovesicular fatty changes

Among the C57BL/6JBomTac mice, only one of the scored histological features significantly differed between the *Lrig3* genotypes; that is, C57BL/6JBomTac *Lrig3 -/-* mice had lower scores for hepatocellular macrovesicular steatosis in the liver ($p = 0.0002$, Kruskal–Wallis test) (Fig. 2B, C) than both *Lrig3*+/+ mice ($p = 0.0011$, post hoc Dunn's comparison) and *Lrig3*+/- mice ($p = 0.0010$, post hoc Dunn's comparison). In the 129S1-U mice, the results revealed a similar but nonsignificant trend toward lower scores for hepatocellular macrovesicular steatosis among the *Lrig3-/-* mice (Kruskal–Wallis test, $p = 0.103$). We also performed binary logistic regression analyses using a five-tiered scoring method, where scores of 0 (normal) and 1 (minimal) were classified as "no hepatocellular steatosis," and the remaining scores (2, 3, and 4, for mild, moderate, and severe, respectively) were classified as hepatocellular steatosis. In the simple analysis, which included only *Lrig3* genotype, the effect of the *Lrig3-/-* genotype on hepatocellular macrovesicular steatosis was significant (Table 2, $p = 0.0028$). To correct for the effect of body weight, a second model that included both

Table 1
Significant differences ($p < 0.01$) between *Lrig3* genotypes in the C57BL/6JBomTac and 129S1-U mouse strains ranked according to their significance levels.[a]

Phenotype	p value[b]		Post hoc discovery[c]	Post hoc significance[c]	
	C57BL/6JBomTac	129S1		C57BL/6JBomTac	129S1
Body weight	< 0.0001	< 0.0001	ko reduced compared to wt and hz	< 0.0001, < 0.0001	0.0013, 0.0003
Liver, macrovesicular hepatocellular steatosis	0.0002	0.103	ko reduced compared to wt and hz	0.0011, 0.0010	-
Ileum dilation	0.417	0.001	ko increased compared to wt and hz	-	0.004, 0.006
Middle ear infiltrate, foamy macrophages and neutrophils	0.749	0.005	ko increased compared to wt and hz	-	0.0055, 0.0420

[a] The complete list of all analyzed histopathologies is provided in Supplementary Table 2.
[b] P-value according to the Kruskal–Wallis test for categorical data and Student's *t*-test for numerical data.
[c] According to Dunn's comparison for categorical data and Tukey's multiple comparisons for numerical data. Abbreviations: ko, knockout (*Lrig3 -/-);* wt, wild type (*Lrig3 +/+);* hz, heterozygote (*Lrig3 +/-).*

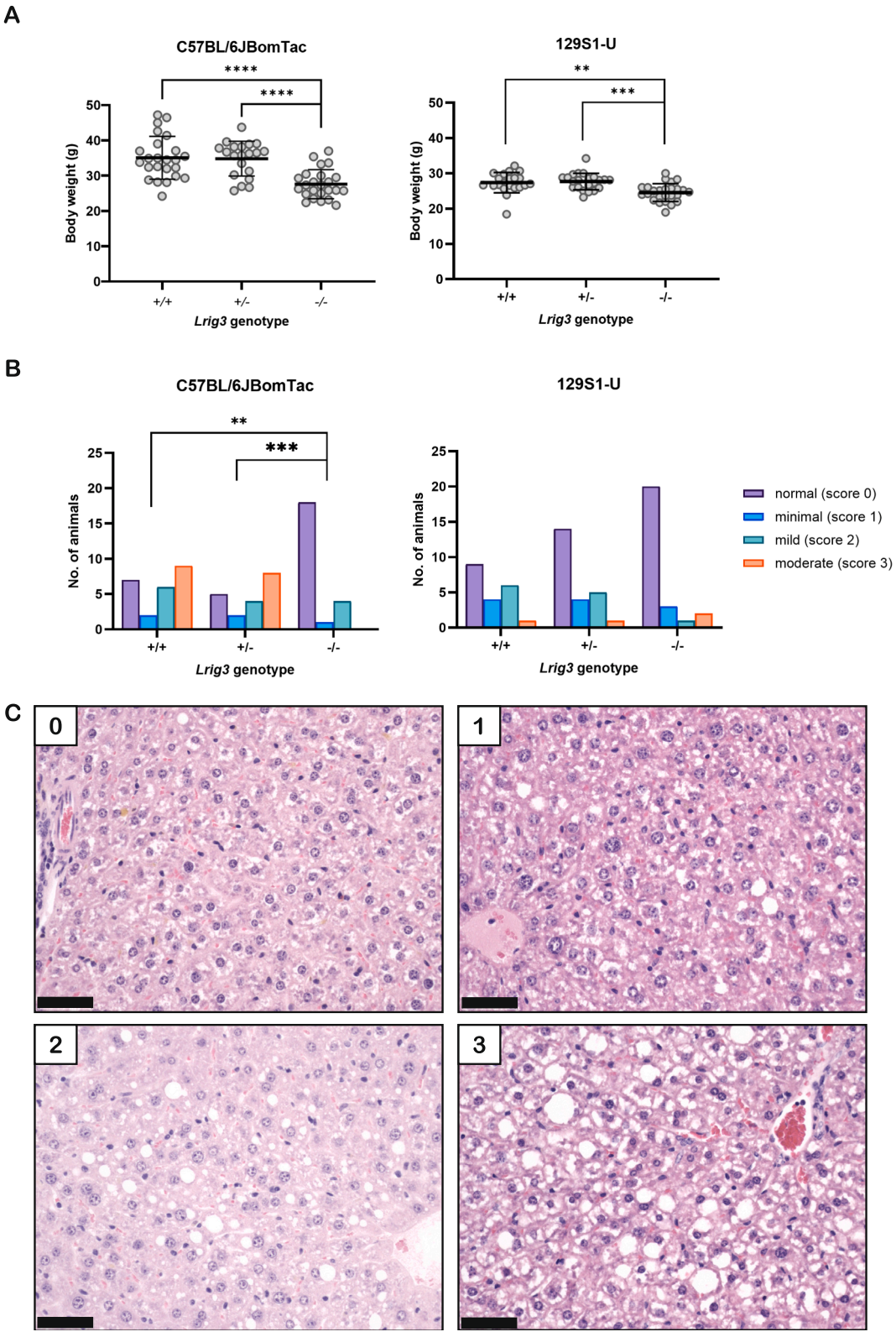

Fig. 2. Body weights and fatty liver scores of C57BL/6JBomTac and 129S1-U mice with different *Lrig3* genotypes. **A**. Body weights of female C57BL/6JBomTac and 129S1-U mice at 12 months of age. **B**. Distribution of scores for macrovesicular hepatocellular steatosis in female mice sacrificed at 12 months of age according to background strain and *Lrig3* genotype. ** $p < 0.01$, *** $p < 0.001$ (Student's *t*-test with Tukey's multiple comparisons). **C.** Representative hematoxylin and eosin-stained histomicrographs of macrovesicular hepatocellular steatosis in female mice sacrificed at 12 months of age. The scale bar indicates 50 μm. (0) No macrovesicular hepatocellular steatosis, (1) minimal macrovesicular hepatocellular steatosis, (2) mild macrovesicular hepatocellular steatosis, and (3) moderate macrovesicular hepatocellular steatosis. No animal had a severe score (4). The scale bar indicates 200 μm.

Table 2
Logistic regression analysis results for the probability of macrovesicular hepatocellular degeneration without and with respect to body weight.

		C57BL/6JBomTac			129S1-U		
		Odds ratio	**95% confidence interval**	**p value**	**Odds ratio**	**95% confidence interval**	**p value**
Model with genotype only	*Lrig3*+/+	1			1		
	Lrig3+/-	1.03	0.30-3.57	0.9646	0.62	0.17-2.28	0.4707
	Lrig3-/-	0.13	0.03-0.49	0.0028*	0.24	0.05-1.10	0.0664
Model with genotype and body weight	*Lrig3*+/+	1			1		
	Lrig3+/-	1.01	0.26-3.90	0.9850	0.46	0.11-1.89	0.2850
	Lrig3-/-	0.32	0.07-1.47	0.1423	0.40	0.08-2.12	0.2801
	Body weight	1.18	1.04-1.34	0.0094*	1.23	0.95-1.59	0.1091

* $p < 0.05$.

genotype and body weight was analyzed. In this model, only body weight had a significant effect on the risk of developing hepatocellular macrovesicular steatosis (Table 2, $p = 0.0094$), whereas the effect of the *Lrig3*-/- genotype was non-significant (Table 2, $p = 0.1423$).

3.5. *Lrig3*-deficient 129S1-U mice presented an increased incidence of ileum dilation, with no changes in intestinal wall thickness

At necropsy, some animals were observed to have dilated gastrointestinal sections (Fig. 3A and B), including the esophagus and different parts of the intestines, most commonly the small intestine. In 129S1-U mice, a dilated ileum was more common in *Lrig3* -/- mice than in *Lrig3*+/+ and Lrig3+/- mice ($p = 0.004$ and $p = 0.005$, respectively, post hoc Dunn's multiple comparison test).

In a preliminary report, *Lrig3* expression was reported to play a role in the cellular census of the colonic crypt (Stevenson et al., 2022). We therefore investigated whether *Lrig3* genotype affected intestinal wall thicknesses in the two mouse strains by measuring the thickness of the intestinal mucosa, crypt, and muscularis (Fig. 3E). Two areas in the jejunum, ileum, and colon were measured in each animal. This analysis did not reveal any differences in mucosal, crypt, or muscularis thickness between the *Lrig3* genotypes (one-way analysis of variance [ANOVA] with Tukey's multiple comparisons test, Supplementary Table 3).

3.6. *Lrig3*-deficient 129S1-U mice presented an increased incidence of inflammatory cell infiltrates in the middle ear

Compared with 129S1-U *Lrig3* +/+ mice ($p = 0.0055$) and 129S1-U *Lrig3* +/- mice ($p = 0.00420$), 129S1-U *Lrig3* -/- mice presented with an increased incidence of inflammatory cell infiltrate in the middle ear (Table 1 and Fig. 4). A single C57BL/6JBomTac *Lrig3*-/- mouse presented with a moderate middle ear neutrophilic inflammation with hemorrhage and edema (acute purulent otitis media). In all other animals with inflammatory cell infiltrate, there was no edema, congestion, hemorrhage, or necrosis.

3.7. *Lrig3* genotype did not correlate with tumor incidence

A previous study indicated that *Lrig3*-deficient mice might develop abdominal tumors at a relatively increased rate (Hellström et al., 2016). However, there was no difference in tumor incidence between mice with different *Lrig3* genotypes (Table 3). The only tumors found in the 140 mice analyzed were lymphomas and pulmonary adenomas, many of which were small and required histopathological examination for diagnosis. The C57BL/6JBomTac mice had a high incidence of tumors: 58 %, 70 %, and 79 % for the *Lrig3*+/+, *Lrig3*+/-, and *Lrig3*-/- genotypes, respectively. The most common tumor in C57BL/6JBomTac mice was lymphoma in Peyer's patches, followed by lymphoma in the lymph nodes, lymphoma in the spleen, and pulmonary adenoma. Only five 129S1-U mice were diagnosed with tumors, four with pulmonary adenomas and two with lymphomas.

3.8. High-fat diet-fed *Lrig3*-deficient C57BL/6JBomTac mice presented with reduced incidence of hepatocellular microvesicular fatty changes

Because female *Lrig3*-/- C57BL/6JBomTac mice were protected against spontaneous macrovesicular hepatocellular changes at one year of age, we investigated whether they were also protected against fatty liver induced by a HFD. 129S1-U mice were not included in this experiment because they did not exhibit a clear liver phenotype in the original histopathological examination. Eight-week-old female and male C57BL/6JBomTac mice with different *Lrig3* genotypes were fed a HFD for eight weeks. Here, we included both males and females to account for sex differences in metabolic control and regulation. After 8 weeks of consuming a HFD, both female and male mice of each of the three *Lrig3* genotypes presented increased body weights, increased proportions of fatty tissue, and decreased proportions of lean tissue (Fig. 5). However, there was no difference between the *Lrig3* genotypes of either sex with respect to body weights, proportions of fatty or lean tissue, tibia lengths, liver weights, or gonadal fat pad weights at the end of the eight-week HFD regimen (Supplementary Table 4). There were no effects of *Lrig3* genotype on insulin or glucose levels, or across a large panel of hematology and clinical chemistry parameters, in either sex (Supplementary Table 4). At the end of the eight-week HFD regimen, histopathological examination of the livers revealed reductions in microvesicular hepatocyte changes in female *Lrig3*-/- mice compared with female *Lrig3*+/+ mice ($p = 0.022$, Kruskal–Wallis test with Dunn's multiple comparison test) (Fig. 6A). Compared with one-year-old mice, which presented with very few microvesicular hepatocyte changes, the HFD-fed mice presented with increased occurrences of microvesicular hepatocyte changes. There were no differences between mice of different *Lrig3* genotypes in macrovesicular degeneration of hepatocytes in the HFD experiment (Fig. 6B), and the scores were generally lower in the HFD-fed mice than in the 1-year-old mice.

4. Discussion

In this study, we performed an unbiased and extensive histopathological examination of 1-year-old mice of different *Lrig3* genotypes with two different genetic backgrounds: C57BL/6JBomTac and 129S1-U. In the primary screen, we observed four significant ($p < 0.01$) effects of *Lrig3* expression ablation: (i) an age-dependent reduction in body weight in C57BL/6JBomTac and 129S1-U mice; (ii) a reduced incidence of hepatocellular macrovesicular steatosis in C57BL/6JBomTac mice; (iii) an increased occurrence of dilated ileum in 129S1-U mice; and (iv) an increased incidence of inflammatory cells infiltrating the middle ear of 129S1-U mice. The presence of both strain-independent and strain-dependent phenotypes highlights the importance of considering the genetic background when investigating the function of *Lrig3* expression in mice.

Strain-dependent phenotypes are usually attributed to the presence of modifier genes that influence the function of the investigated gene (Nadeau, 2001). *Lrig1* and *Ntn1* are two candidate modifier genes of

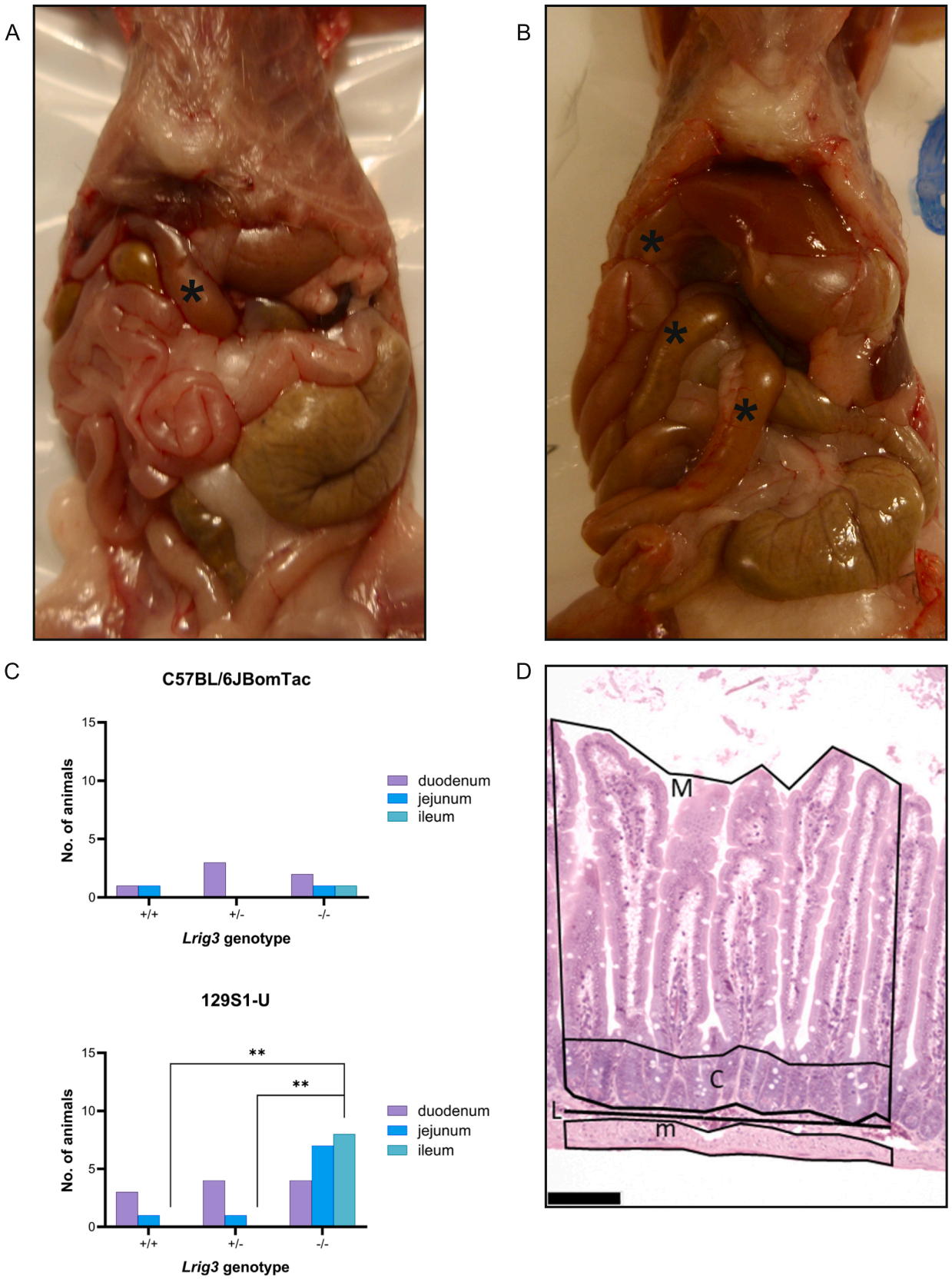

Fig. 3. Intestinal dilations and intestinal morphology in C57BL/6JBomTac and 129S1-U mice with different *Lrig3* genotypes. **A**. Representative photograph of a 129S1-U mouse with a dilated duodenum (asterisk), whereas the other intestinal parts were within the normal range. **B**. Representative photograph of a 129S1-U mouse with a dilated duodenum and jejunum (asterisks), whereas the other intestinal parts were within the normal range. **C**. Bar charts of the number of C57BL/6JBomTac and 129S1-U mice with dilated small intestine segments. **D**. Histomicrograph of a hematoxylin and eosin-stained ileum illustrating how the mucosal areas (M), crypt areas (C), and muscularis areas (m) were measured. **p < 0.01 (ANOVA with Tukey's multiple comparisons). The scale bar indicates 50 μm.

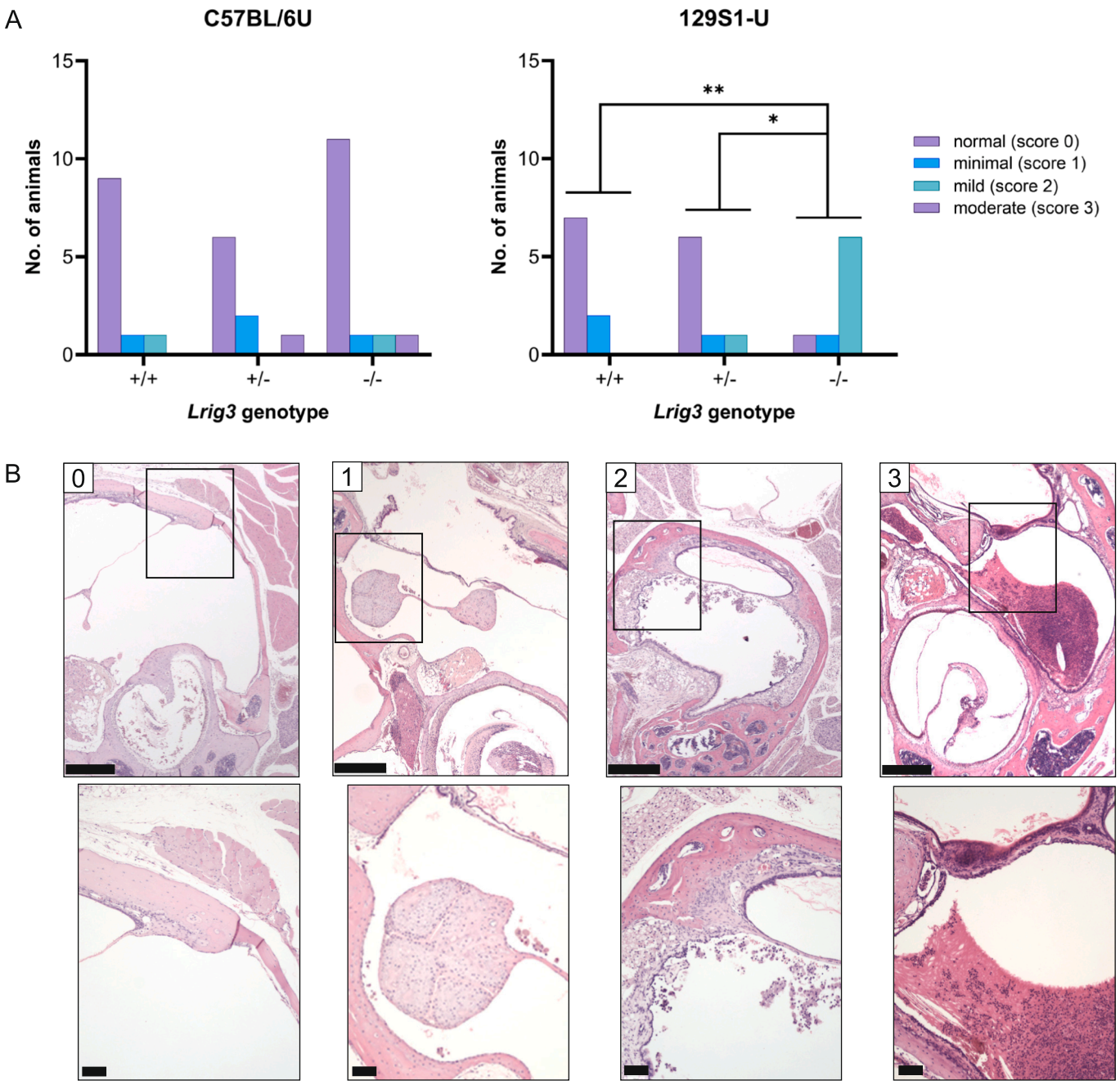

Fig. 4. Inflammatory cell infiltrate in the middle ear of C57BL/6JBomTac and 129S1-U mice of different *Lrig3* genotypes. **A**. Bar charts showing the number of animals with inflammatory cell infiltrate in the middle ear, ** = $p < 0.01$, * $p < 0.05$ (Kruskal–Wallis with Dunn's post-hoc comparisons). **B**. Representative hematoxylin and eosin-stained histomicrographs of the middle ears of female mice sacrificed at 12 months of age with scores of (0) normal, (1) minimal, (2) mild, and (3) moderate inflammatory cellular infiltrate. No animal had a severe score (4). The scale bar indicates 200 μm in the upper row and 50 μm in the lower row (insets).

Table 3
Tumor frequencies in one-year old female mice with different *Lrig3* genotypes. The number of animals with tumors (% of mice) is indicated. Each animal could have more than one tumor.

	C57BL/6JBomTac			129S1-U		
	Lrig3+/+ (n = 24)	*Lrig3*+/- (n = 20)	*Lrig3*-/- (n = 24)	*Lrig3*+/+ (n = 22)	*Lrig3*+/- (n = 24)	*Lrig3*-/- (n = 26)
Lymphoma, Peyer's patches	8 (33)	9 (45)	10 (42)	0	0	0
Lymphoma, spleen	6 (25)	3 (15)	4 (17)	1 (5)	0	1 (4)
Lymphoma, lymph node	9 (38)	11 (55)	12 (50)	0	0	0
Total number of mice with lymphoma	14 (58)	14 (70)	19 (79)	1 (5)	0	1 (4)
Pulmonary adenoma	1 (4)	1 (4)	1 (4)	2 (9)	1 (4)	1 (4)
Total number of mice with at least one tumor	14 (58)	14 (70)	19 (79)	3 (14)	1 (4)	1 (4)

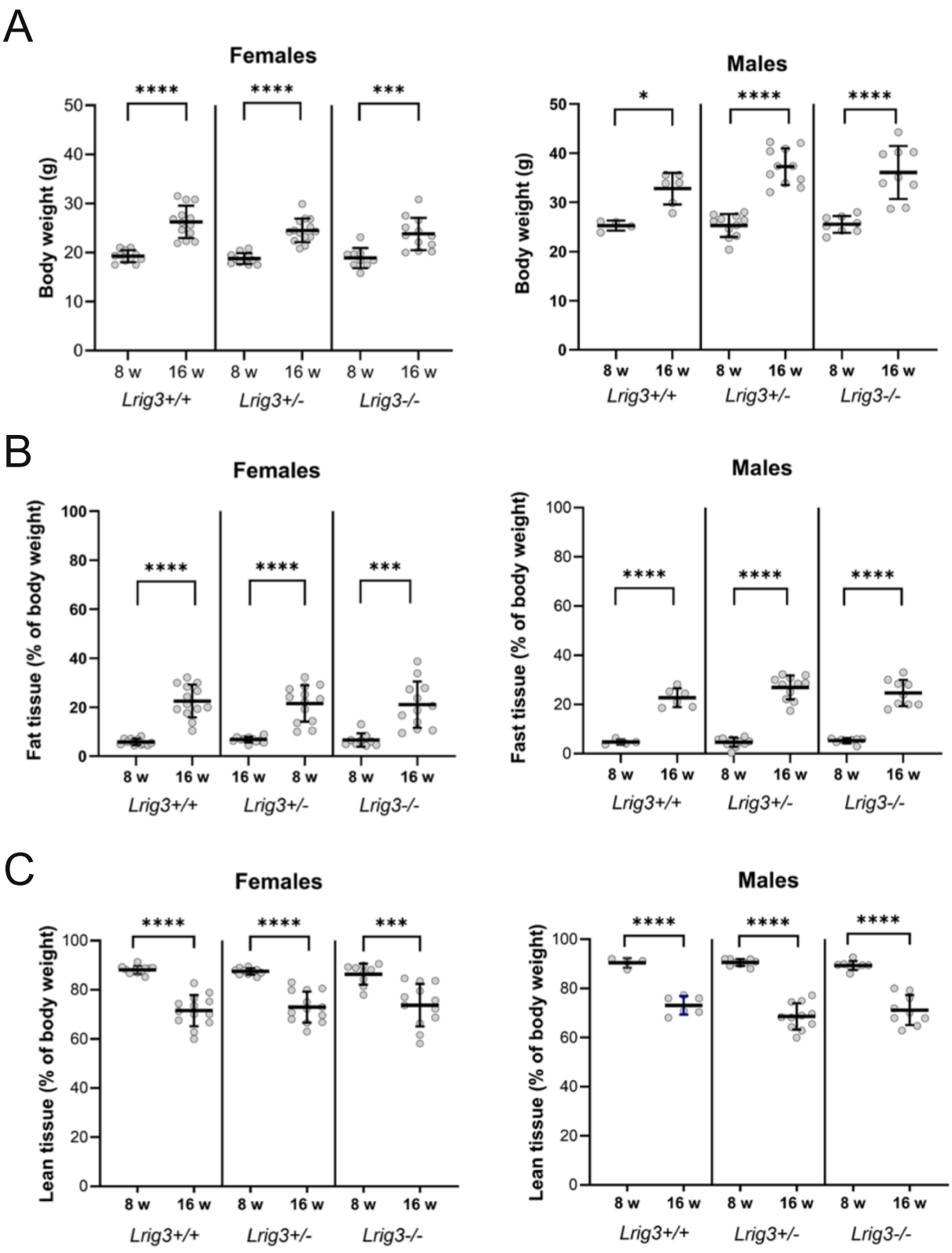

Fig. 5. Body weights and proportions of fatty and lean tissues in female and male C57BL/6JBomTac mice of different *Lrig3* genotypes before and after eight weeks of high-fat diet treatment starting at 8 weeks of age. **A.** Body weights of different *Lrig3* genotypes at the indicated ages. **B.** Proportion of fatty tissue in mice with different *Lrig3* genotypes measured using an Echo-MRI 100 system at the indicated ages. **C.** Proportions of lean tissue in mice with different *Lrig3* genotypes measured using an Echo-MRI 100 system at the indicated ages. * $p < 0.05$, *** $p < 0.001$, *** $p < 0.0001$, Student's *t* test with post hoc Tukey comparisons.

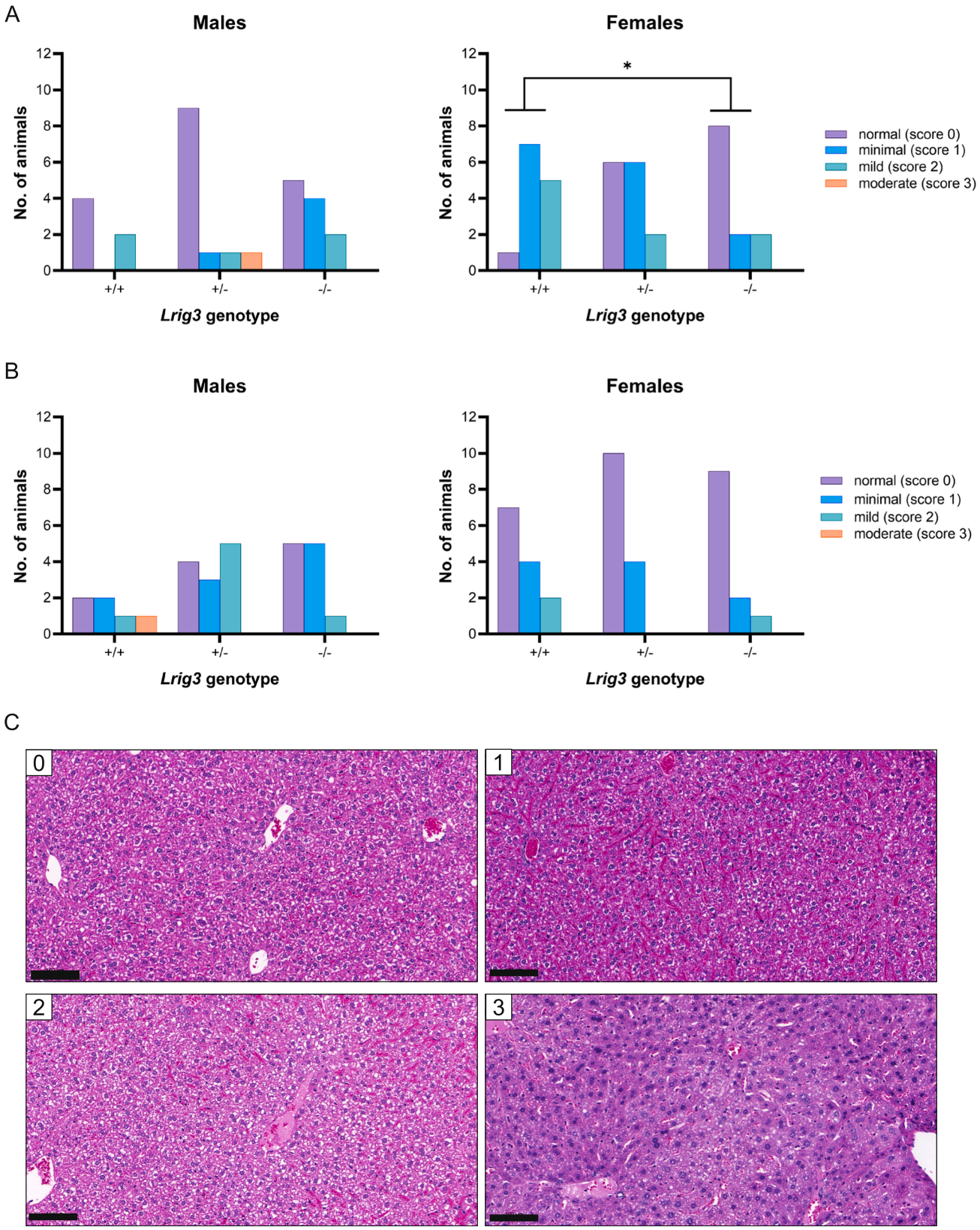

Fig. 6. Vesicular hepatocellular degenerative changes in C57BL/6JBomTac female and male mice of different *Lrig3* genotypes after eight weeks of high-fat diet treatment starting at 8 weeks of age. **A.** Number of animals with different scores of microvesicular hepatocellular degenerative change. **B.** Number of animals with different macrovesicular hepatocellular degenerative change scores. **C** Representative hematoxylin and eosin-stained histomicrographs of microvesicular hepatocellular steatosis after eight weeks of high-fat diet treatment. The slides were stained with hematoxylin and eosin. (0) No microvesicular hepatocellular steatosis, (1) minimal microvesicular hepatocellular steatosis, (2) mild microvesicular hepatocellular steatosis, and (3) moderate microvesicular hepatocellular steatosis. No animal had a severe score (4). The scale bar indicates 50 μm. * $p < 0.05$, Kruskal–Wallis with post hoc Dunn's comparisons.

Lrig3. *Lrig1* and *Lrig3* have been suggested to have redundant functions and to compensate for one another during inner ear development (Del Rio et al., 2013) and for sensory axonal growth (De Vincenti et al., 2021). In fact, we recently showed that LRIG1 and LRIG3 redundantly sensitize cells to low concentrations of BMP (Herdenberg et al., 2021). *Ntn1*, encoding netrin-1, counteracts the function of *Lrig3* during inner ear development (Abraira et al., 2008). Intriguingly, whereas LRIG1 and LRIG3 promote BMP signaling (Herdenberg et al., 2021; Abdullah et al., 2023), netrin-1 suppresses the same signaling pathway (Abdullah et al., 2021). Therefore, we expect that other genes that regulate various aspects of BMP signaling might also emerge as phenotypic modifiers of *Lrig3*.

In this study, ablation of *Lrig3* expression in C57BL/6JBomTac mice caused an age-related body weight reduction in 12-month-old female mice but not in 8- or 16-week-old female mice. The lack of differences in body weight up to 16 weeks of age is consistent with data from the mouse phenotype consortium, which indicate that male and female *Lrig3*-/- C57BL/6NCrl mice have body weights similar to those of their *Lrig3*+/+ counterparts (https://www.mousephenotype.org). In principle, reduced body weight could suggest reduced food intake, reduced nutritional uptake, or increased metabolic rate. However, in the current study, we did not monitor food intake or energy expenditure. Therefore, the reason for the age-dependent reduction in body weight among the *Lrig3*-/- mice remains to be investigated.

One-year-old female *Lrig3*-/- C57BL/6JBomTac mice presented a body weight-dependent reduction in the incidence of spontaneous hepatocellular macrovesicular steatosis. In the preliminary analysis (Herdenberg 2021), which used a four-tiered scoring method, the effect of the *Lrig3*-/- genotype was significant also when body weight was included in the binary logistic regression analysis. Here, however, where we used a slightly different five-tiered scoring method, the effect of the *Lrig3*-/- genotype became non-significant when body weight was included in the analysis. Therefore, on the basis of the divergent analysis results between the preliminary and current studies, we could not conclude whether *Lrig3* genotype was an independent predictive factor for the risk of steatosis. Regarding the ability of Lrig3 to promote BMP signaling (Herdenberg et al., 2021; Abullah et al., 2023), it is notable that BMP signaling has been implicated in the etiology of hepatic steatosis both in mice and men (Thayer et al., 2020; Vacca et al., 2020). However, to determine the causal links between *Lrig3* and hepatic steatosis, further investigations are needed. In the HFD experiment, *Lrig3*-/- mice presented a lower incidence of microvesicular hepatocellular degeneration, or microvesicular steatosis, than the corresponding *Lrig3*+/+ mice. In mice, microvesicular steatosis usually indicates either more severe hepatic dysfunction or nutritional imbalance than macrovesicular hepatocellular degeneration does (Thoolen et al., 2010), although it is also an intermediate stage of macrovesicular hepatocellular degeneration (Kristiansen et al., 2019). In any case, the reduced incidence of microvesicular steatosis observed in *Lrig3*-/- mice was clearly independent of body weight because the *Lrig3* genotypes did not differ in body weight before or after the 8-week HFD regimen.

One-year-old female *Lrig3*-deficient 129S1-U mice exhibited an increased incidence of ileum dilation but no changes in the mucosal thickness of any of the intestinal segments analyzed. *Lrig3* expression has been suggested to regulate the colonic stem cell compartment, resulting in increased colon mucosal thickness at 6–10 weeks of age (Stevenson et al., 2022). Therefore, the results of the present study may indicate an age-dependent role of *Lrig3* expression in the regulation of colonic stem cells and mucosal morphology. *Lrig1*-deficient mice also present an intestinal phenotype caused by the hyperproliferation of intestinal stem cells (Wong et al., 2012; Powell et al., 2012), possibly through the promotion of BMP signaling (Herdenberg and Hedman, 2023). Therefore, as discussed earlier, expression of the intact *Lrig1* gene might be able to compensate for that of the ablated *Lrig3* gene. BMP signaling has been reported to be important for the differentiation of enterocytes along the villus axis (Beumer et al., 2022; Kraiczy et al., 2023), and investigating whether *Lrig3*, *Lrig1*, or both are involved in the regulation of enterocyte differentiation would therefore be interesting.

One-year-old female *Lrig3*-deficient 129S1-U mice also presented an increased incidence of middle ear inflammatory infiltrate. This can occur spontaneously, often due to a breach or compromise in the natural barriers of the middle ear, and is not necessarily caused by infection (Ramos et al., 2018; Verdaguer et al., 2006). The pathogenesis behind this condition is unknown. Therefore, although *Lrig3* apparently plays an important role in this process, it remains difficult to address the exact role of *Lrig3* in middle ear inflammation.

The present study was partly motivated by our preliminary observation that *Lrig3*-deficient C57BL/6JBomTac mice tend to form abdominal tumors at an increased rate compared with their wild-type littermates (Hellström et al., 2016). *Lrig1*-deficient mice spontaneously develop duodenal tumors (Powell et al., 2012), and *Lrig1* functions as a haploinsufficient tumor suppressor in experimental glioma in mice (Mao et al., 2018), whereas *Lrig2*-deficient mice are protected against experimental glioma (Rondahl et al., 2013). There was no difference in tumor incidence between mice of different *Lrig3* genotypes, and the tumor types identified were those that have been reported as the most common in the two mouse strains used – lymphoma, especially of Peyer's patches, in C57BL/6 strains; and pulmonary adenoma in 129 strains (Cooper et al 2021; Brayton et al 2012). To address the potential role of *Lrig3* in tumor development, it might be appropriate to use a more tumor-prone mouse strain, analyze mice of older age, or expose the mice to carcinogenic insults.

This study has several limitations. One limitation is that the study was mostly descriptive, and thus, it did not provide extensive mechanistic insight. However, a thorough phenotypic description of *Lrig3* mutant mice will serve as the basis for further mechanistic studies. Another limitation is that the histopathological examination was performed only on one-year-old female mice. Hence, we might have missed phenotypes that become apparent only at older ages or earlier in development or only in male mice. For example, cancer development might be better studied with older mice or under other environmental conditions.

In summary, we showed both strain-independent and strain-dependent effects of *Lrig3* ablation in two different mouse strains. It remains to be determined whether the Lrig3-mediated regulation of BMP signaling, or other functions of *Lrig3*, affects body weight, liver steatosis, intestinal morphology, and middle ear inflammation. In this context, determining the strain-specific genetic modifiers that influence the physiological function of *Lrig3* is important.

CRediT authorship contribution statement

Carl Herdenberg: Writing – review & editing, Writing – original draft, Visualization, Validation, Methodology, Investigation, Formal analysis, Data curation, Conceptualization. **Roger Henriksson:** Writing – review & editing, Supervision, Resources, Funding acquisition, Conceptualization. **Håkan Hedman:** Writing – review & editing, Writing – original draft, Validation, Supervision, Resources, Project administration, Methodology, Funding acquisition, Formal analysis, Data curation, Conceptualization. **Veronica Rondahl:** Writing – review & editing, Visualization, Validation, Supervision, Methodology, Investigation, Formal analysis, Data curation, Conceptualization.

Data availability

All DNA sequencing data were deposited in the European Nucleotide Archive (ENA) under the accession number PRJEB82724 (https://www.ebi.ac.uk/ena/browser/text-search?query=PRJEB82724). The PCR primer and probe sequences were deposited in the Open Science Framework (OSF), DOI https://doi.org/10.17605/OSF.IO/586K9, as Supplementary Table 1 (https://osf.io/4ts2x). All histopathology scores were deposited in the OSF, DOI https://doi.org/10.17605/OSF.IO/

586K9, as Supplementary Table 2 (https://osf.io/r3ehz). All intestinal mucosa and muscularis thickness and villi height measurements were deposited in the OSF, DOI https://doi.org/10.17605/OSF.IO/586K9, as Supplementary Table 3 (https://osf.io/amh32). Body, liver and gonadal fat pad weights, tibia lengths, Echo-MRI results, and serum clinical chemistry results were deposited in the OSF, DOI https://doi.org/10.17605/OSF.IO/586K9, as Supplementary Table 4 (https://osf.io/7hjxp).

Declaration of competing interest

The authors declare that they have no known competing financial interests or personal relationships that could have appeared to influence the work reported in this paper.

Acknowledgments

We thank Sigrid Kilter, Yvonne Jonsson, Charlotte Nordström, and Annika Holmberg at Umeå University and Ulrika Larsson-Petterson at the National Veterinary Institute for excellent technical assistance and Björn Tavelin for statistical advice. DNA sequencing was performed by the SNP&SEQ Technology Platform in Uppsala, Sweden. This facility is part of the National Genomics Infrastructure (NGI) Sweden and Science for Life Laboratory. The SNP&SEQ Platform is also supported by the Swedish Research Council and the Knut and Alice Wallenberg Foundation. The computations and data handling were enabled by resources provided by the National Academic Infrastructure for Supercomputing in Sweden (NAISS), partially funded by the Swedish Research Council through grant agreement no. 2022-06725. Support by NBIS (National Bioinformatics Infrastructure Sweden) is also gratefully acknowledged. This work was supported by grants from the Swedish Cancer Society (CAN 2018/546), the Kempe Foundation (JCK-1829), the Cancer Research Foundation in Northern Sweden (AMP 16–799), Lion's Cancer Research Foundation at Umeå University (LP 16–2134 and LP 15–2057), and the regional agreement between Umeå University and the Västerbotten County Council for cooperation in the fields of medicine, odontology and health (ALF, RV 836951). Veronica Rondahl was supported by a grant from the Swedish Research Council (522-2009-5838) while working at the National Veterinary Institute.

Appendix A. Supplementary data

Supplementary data to this article can be found online at https://doi.org/10.1016/j.gene.2025.149539.

References

Abdullah, A., Herdenberg, C., Hedman, H., 2023. Ligand-specific regulation of transforming growth factor beta superfamily factors by leucine-rich repeats and immunoglobulin-like domains proteins. PLoS One 18 (8), e0289726. https://doi.org/10.1371/journal.pone.0289726 eCollection 2023. PMID: 37603563.

Abdullah, A., Herdenberg, C., Hedman, H., 2021. Netrin-1 functions as a suppressor of bone morphogenetic protein (BMP) signaling. Sci. Rep. 11 (1), 8585. https://doi.org/10.1038/s41598-021-87949-7. PMID: 33883596.

Abousoliman, I., Reyer, H., Oster, M., Murani, E., Mohamed, I., Wimmers, K., 2021. Genome-wide analysis for early growth-related traits of the locally adapted egyptian Barki Sheep. Genes (Basel) 12 (8), 1243. https://doi.org/10.3390/genes12081243. PMID: 34440417.

Abraira, V.E., Del Rio, T., Tucker, A.F., Slonimsky, J., Keirnes, H.L., Goodrich, L.V., 2008. Cross-repressive interactions between Lrig3 and netrin 1 shape the architecture of the inner ear. Development 135 (24), 4091–4099. https://doi.org/10.1242/dev.029330. Epub 2008 Nov 12 PMID: 19004851.

Akey, J.M., Ruhe, A.L., Akey, D.T., Wong, A.K., Connelly, C.F., Madeoy, J., Nicholas, T.J., Neff, M.W., 2010. Tracking footprints of artificial selection in the dog genome. PNAS 107 (3), 1160–1165. https://doi.org/10.1073/pnas.0909918107. Epub 2010 Jan 11 PMID: 20080661.

Beumer, J., Puschhof, J., Yengej, F.Y., Zhao, L., Martinez-Silgado, A., Blotenburg, M., Begthel, H., Boot, C., van Oudenaarden, A., Chen, Y.G., Clevers, H., 2022. BMP gradient along the intestinal villus axis controls zonated enterocyte and goblet cell states. Cell Rep. 38 (9), 110438. https://doi.org/10.1016/j.celrep.2022.110438. PMID: 35235783.

Brayton, C.F., Treuting, P.M., Ward, J.M., 2012. Pathobiology of aging mice and GEM: background strains and experimental design. Vet. Pathol. 49 (1), 85–105. https://doi.org/10.1177/0300985811430696. PMID: 22215684 Review.

Cooper, T.K., Meyerholz, D.K., Beck, A.P., Delaney, M.A., Piersigilli, A., Southard, T.L., Brayton, C.F., 2021. Research-relevant conditions and pathology of laboratory mice, rats, gerbils, guinea pigs, hamsters, naked mole rats, and rabbits. ILAR J. 62 (1–2), 77–132. https://doi.org/10.1093/ilar/ilab022. PMID: 34979559.

De Vincenti, A.P., Alsina, F.C., Ferrero Restelli, F., Hedman, H., Ledda, F., Paratcha, G., 2021. Lrig1 and Lrig3 cooperate to control Ret receptor signaling, sensory axonal growth and epidermal innervation. Development 148 (16), dev197020. https://doi.org/10.1242/dev.197020. Epub 2021 Aug 12. PMID: 34338291.

Del Rio, T., Nishitani, A.M., Yu, W.M., Goodrich, L.V., 2013. In vivo analysis of Lrig genes reveals redundant and independent functions in the inner ear. PLoS Genet. 9 (9), e1003824. https://doi.org/10.1371/journal.pgen.1003824. Epub 2013 Sep 26. PMID: 24086156.

Dickinson, M.E., Flenniken, A.M., Ji, X., Teboul, L., Wong, M.D., White, J.K., Meehan, T. F., Weninger, W.J., Westerberg, H., Adissu, H., Baker, C.N., Bower, L., Brown, J.M., Caddle, L.B., Chiani, F., Clary, D., Cleak, J., Daly, M.J., Denegre, J.M., Doe, B., Dolan, M.E., Edie, S.M., Fuchs, H., Gailus-Durner, V., Galli, A., Gambadoro, A., Gallegos, J., Guo, S., Horner, N.R., Hsu, C.W., Johnson, S.J., Kalaga, S., Keith, L.C., Lanoue, L., Lawson, T.N., Lek, M., Mark, M., Marschall, S., Mason, J., McElwee, M.L., Newbigging, S., Nutter, L.M., Peterson, K.A., Ramirez-Solis, R., Rowland, D.J., Ryder, E., Samocha, K.E., Seavitt, J.R., Selloum, M., Szoke-Kovacs, Z., Tamura, M., Trainor, A.G., Tudose, I., Wakana, S., Warren, J., Wendling, O., West, D.B., Wong, L., Yoshiki, A., International Mouse Phenotyping Consortium, Jackson Laboratory Infrastructure Nationale PHENOMIN, Institut Clinique de la Souris (ICS), Charles River Laboratories, MRC Harwell, Toronto Centre for Phenogenomics, Wellcome Trust Sanger Institute, RIKEN BioResource Center, MacArthur, D.G., Tocchini-Valentini, G.P., Gao, X., Flicek, P., Bradley, A., Skarnes, W.C., Justice, M.J., Parkinson, H.E., Moore, M., Wells, S., Braun, R.E., Svenson, K.L., de Angelis, M.H., Herault, Y., Mohun, T., Mallon, A.M., Henkelman, R.M., Brown, S.D., Adams, D.J., Lloyd, K.C., McKerlie, C., Beaudet, A.L., Bućan, M., Murray, S.A., 2016. High-throughput discovery of novel developmental phenotypes. Nature 537 (7621), 508–514. https://doi.org/10.1038/nature19356. Epub 2016 Sep 14. PMID: 27626380.

Faraz, M., Herdenberg, C., Holmlund, C., Henriksson, R., Hedman, H., 2018. A protein interaction network centered on leucine-rich repeats and immunoglobulin-like domains 1 (LRIG1) regulates growth factor receptors. J. Biol. Chem. 293 (9), 3421–3435.

Groza, T., Gomez, F.L., Mashhadi, H.H., Muñoz-Fuentes, V., Gunes, O., Wilson, R., Cacheiro, P., Frost, A., Keskivali-Bond, P., Vardal, B., McCoy, A., Cheng, T.K., Santos, L., Wells, S., Smedley, D., Mallon, A.M., Parkinson, H., 2023. The International Mouse Phenotyping Consortium: comprehensive knockout phenotyping underpinning the study of human disease. Nucleic Acids Res. 51 (D1), D1038–D1045. https://doi.org/10.1093/nar/gkac972. PMID: 36305825.

Guo, D., Holmlund, C., Henriksson, R., Hedman, H., 2004. The LRIG gene family has three vertebrate paralogs widely expressed in human and mouse tissues and a homolog in Ascidiacea. Genomics 84 (1), 157–165.

Gur, G., Rubin, C., Katz, M., Amit, I., Citri, A., Nilsson, J., Amariglio, N., Henriksson, R., Rechavi, G., Hedman, H., Wides, R., Yarden, Y., 2004. LRIG1 restricts growth factor signaling by enhancing receptor ubiquitylation and degradation. EMBO J. 23 (16), 3270–3281.

Hellström, M., Ericsson, M., Johansson, B., Faraz, M., Anderson, F., Henriksson, R., Nilsson, S.K., Hedman, H., 2016. Cardiac hypertrophy and decreased high-density lipoprotein cholesterol in Lrig3-deficient mice. Am. J. Physiol. Regul. Integr. Comp. Physiol. 310 (11), R1045–R1052. https://doi.org/10.1152/ajpregu.00309.2015. Epub 2016 PMID: 27009049.

Herdenberg, C., 2021. Molecular and physiological functions of LRIG proteins and netrin-1 in health and disease [dissertation]. Umeå (Sweden): Umeå Universitet. Available at: http://umu.diva-portal.org/smash/get/diva2:1587443/FULLTEXT01.pdf.

Herdenberg, C., Mutie, P.M., Billing, O., Abdullah, A., Strawbridge, R.J., Dahlman, I., Tuck, S., Holmlund, C., Arner, P., Henriksson, R., Franks, P.W., Hedman, H., 2021. LRIG proteins regulate lipid metabolism via BMP signaling and affect the risk of type 2 diabetes. Commun. Biol. 4 (1), 90. https://doi.org/10.1038/s42003-020-01613-w. PMID: 33469151.

Herdenberg, C., Hedman, H., 2023. HYPOTHESIS: Do LRIG proteins regulate stem cell quiescence by promoting BMP signaling? Stem Cell Rev. Rep. 19 (1), 59–66. https://doi.org/10.1007/s12015-022-10442-9. Epub 2022 Aug 15 PMID: 35969315.

Holmlund, C., Nilsson, J., Guo, D., Starefeldt, A., Golovleva, I., Henriksson, R., Hedman, H., 2004. Characterization and tissue-specific expression of human LRIG2. Gene 332, 35–43. https://doi.org/10.1016/j.gene.2004.02.002. PMID: 15145052.

Jensen, K.B., Collins, C.A., Nascimento, E., Tan, D.W., Frye, M., Itami, S., Watt, F.M., 2009. Lrig1 expression defines a distinct multipotent stem cell population in mammalian epidermis. Cell Stem Cell 4 (5), 427–439.

Kraiczy, J., McCarthy, N., Malagola, E., Tie, G., Madha, S., Boffelli, D., Wagner, D.E., Wang, T.C., Shivdasani, R.A., 2023. Graded BMP signaling within intestinal crypt architecture directs self-organization of the Wnt-secreting stem cell niche. Cell Stem Cell 30 (4), 433–449.e8. https://doi.org/10.1016/j.stem.2023.03.004. PMID: 37028407.

Kristiansen, M.N.B., Veidal, S.S., Christoffersen, C., Jelsing, J., Rigbolt, K.T.G., 2019. Molecular characterization of microvesicular and macrovesicular steatosis shows widespread differences in metabolic pathways. Lipids 54 (1), 109–115. https://doi.org/10.1002/lipd.12121. Epub 2019 Feb 5 PMID: 30723896.

Kun, E., Javan, E.M., Smith, O., Gulamali, F., de la Fuente, J., Flynn, B.I., Vajrala, K., Trutner, Z., Jayakumar, P., Tucker-Drob, E.M., Sohail, M., Singh, T., Narasimhan, V. M., 2023. The genetic architecture and evolution of the human skeletal form. Science

381 (6655), eadf8009. https://doi.org/10.1126/science.adf8009. Epub 2023 Jul 21. PMID: 37471560.

Laederich, M.B., Funes-Duran, M., Yen, L., Ingalla, E., Wu, X., Carraway 3rd, K.L., Sweeney, C., 2004. The leucine-rich repeat protein LRIG1 is a negative regulator of ErbB family receptor tyrosine kinases. J. Biol. Chem. 279 (45), 47050–47056. https://doi.org/10.1074/jbc.M409703200. Epub 2004 Sep 1 PMID: 15345710.

Lindquist, D., Kvarnbrink, S., Henriksson, R., Hedman, H., 2014. LRIG and cancer prognosis. Acta Oncol. 53 (9), 1135–1142.

Ma, L., Yang, J., Runesha, H.B., Tanaka, T., Ferrucci, L., Bandinelli, S., Da, Y., 2010. Genome-wide association analysis of total cholesterol and high-density lipoprotein cholesterol levels using the Framingham heart study data. BMC Med. Genet. 11, 55. https://doi.org/10.1186/1471-2350-11-55. PMID: 20370913.

Manichaikul, A., Lin, H., Kang, C., Yang, C., Rich, S.S., Taylor, K.D., Guo, X., Rotter, J.I., Craig Johnson, W., Cornell, E., Tracy, R.P., Peter Durda, J., Liu, Y., Vasan, R.S., Adrienne Cupples, L., Gerszten, R.E., Clish, C.B., Jain, D., Conomos, M.P., Blackwell, T., Papanicolaou, G.J., Rodriguez, A., 2022. Lymphocyte activation gene-3-associated protein networks are associated with HDL-cholesterol and mortality in the Trans-omics for Precision Medicine program. Commun. Biol. 5 (1), 362. https://doi.org/10.1038/s42003-022-03304-0. PMID: 35501457.

Mann, P.C., Vahle, J., Keenan, C.M., Baker, J.F., Bradley, A.E., Goodman, D.G., Harada, T., Herbert, R., Kaufmann, W., Kellner, R., Nolte, T., Rittinghausen, S., Tanaka, T., 2012. International harmonization of toxicologic pathology nomenclature: an overview and review of basic principles. Toxicol. Pathol. 40 (4 Suppl), 7S–13S. https://doi.org/10.1177/0192623312438738. PMID: 22637736 Review.

Mao, F., Holmlund, C., Faraz, M., Wang, W., Bergenheim, T., Kvarnbrink, S., Johansson, M., Henriksson, R., Hedman, H., 2018. Lrig1 is a haploinsufficient tumor suppressor gene in malignant glioma. Oncogenesis. 7 (2), 13. https://doi.org/10.1038/s41389-017-0012-8. PMID: 29391393.

Mekada, K., Yoshiki, A., 2021. Substrains matter in phenotyping of C57BL/6 mice. Exp. Anim. 70 (2), 145–160. https://doi.org/10.1538/expanim.20-0158. Epub 2021 Jan 14 PMID: 33441510.

Metodiev, S., Thekkoot, D.M., Young, J.M., Onteru, S., Rothschild, M.F., Dekkers, J.C.M., 2018. A whole-genome association study for litter size and litter weight traits in pigs. Livest. Sci. 211, 87–97.

Nadeau, J.H., 2001. Modifier genes in mice and humans. Nat. Rev. Genet. 2 (3), 165–174. https://doi.org/10.1038/35056009. PMID: 11256068 Review.

Neirinckx, V., Hedman, H., Niclou, S.P., 2017. Harnessing LRIG1-mediated inhibition of receptor tyrosine kinases for cancer therapy. Biochim. Biophys. Acta 1868 (1), 109–116. https://doi.org/10.1016/j.bbcan.2017.02.007. Epub 2017 Mar 1. PMID: 28259645 Review.

Nilsson, J., Vallbo, C., Guo, D., Golovleva, I., Hallberg, B., Henriksson, R., Hedman, H., 2001. Cloning, characterization, and expression of human LIG1. Biochem. Biophys. Res. Commun. 284 (5), 1155–1161. https://doi.org/10.1006/bbrc.2001.5092. PMID: 11414704.

Óvilo, C., Trakooljul, N., Núñez, Y., Hadlich, F., Murani, E., Ayuso, M., García-Contreras, C., Vázquez-Gómez, M., Rey, A.I., Garcia, F., García-Casco, J.M., López-Bote, C., Isabel, B., González-Bulnes, A., Wimmers, K., Muñoz, M., 2022. SNP discovery and association study for growth, fatness and meat quality traits in Iberian crossbred pigs. Sci. Rep. 12 (1), 16361. https://doi.org/10.1038/s41598-022-20817-0. PMID: 36180572.

Powell, A.E., Wang, Y., Li, Y., Poulin, E.J., Means, A.L., Washington, M.K., Higginbotham, J.N., Juchheim, A., Prasad, N., Levy, S.E., Guo, Y., Shyr, Y., Aronow, B.J., Haigis, K.M., Franklin, J.L., Coffey, R.J., 2012. The pan-ErbB negative regulator Lrig1 is an intestinal stem cell marker that functions as a tumor suppressor. Cell 149 (1), 146–158.

Rafidi, H., Mercado 3rd, F., Astudillo, M., Fry, W.H., Saldana, M., Carraway 3rd, K.L., Sweeney, C., 2013. Leucine-rich repeat and immunoglobulin domain-containing protein-1 (Lrig1) negative regulatory action toward ErbB receptor tyrosine kinases is opposed by leucine-rich repeat and immunoglobulin domain-containing protein 3 (Lrig3). J. Biol. Chem. 288 (30), 21593–21605.

Ramos, M.F., Baker, J., Atzpodien, E.A., Bach, U., Brassard, J., Cartwright, J., Farman, C., Fishman, C., Jacobsen, M., Junker-Walker, U., Kuper, F., Moreno, M.C.R., Rittinghausen, S., Schafer, K., Tanaka, K., Teixeira, L., Yoshizawa, K., Zhang, H., 2018. Nonproliferative and proliferative lesions of the ratand mouse special sense organs(ocular [eye and glands], olfactory and otic). J. Toxicol. Pathol. 31 (3 Suppl), 97S–214S. https://doi.org/10.1293/tox.31.97S. Epub 2018 Jul 28 PMID: 30158741.

Rondahl, V., Holmlund, C., Karlsson, T., Wang, B., Faraz, M., Henriksson, R., Hedman, H., 2013. Lrig2-deficient mice are protected against PDGFB-induced glioma. PLoS One 8 (9), e73635. https://doi.org/10.1371/journal.pone.0073635 eCollection 2013. PMID: 24023893.

Simion, C., Cedano-Prieto, M.E., Sweeney, C., 2014. The LRIG family: enigmatic regulators of growth factor receptor signaling. Endocr. Relat. Cancer 21 (6), R431–R443. https://doi.org/10.1530/ERC-14-0179. Epub 2014 Sep 2 PMID: 25183430.

Smith, N.L., Felix, J.F., Morrison, A.C., Demissie, S., Glazer, N.L., Loehr, L.R., Cupples, L. A., Dehghan, A., Lumley, T., Rosamond, W.D., Lieb, W., Rivadeneira, F., Bis, J.C., Folsom, A.R., Benjamin, E., Aulchenko, Y.S., Haritunians, T., Couper, D., Murabito, J., Wang, Y.A., Stricker, B.H., Gottdiener, J.S., Chang, P.P., Wang, T.J., Rice, K.M., Hofman, A., Heckbert, S.R., Fox, E.R., O'Donnell, C.J., Uitterlinden, A.G., Rotter, J.I., Willerson, J.T., Levy, D., van Duijn, C.M., Psaty, B.M., Witteman, J.C., Boerwinkle, E., Vasan, R.S., 2010. Association of genome-wide variation with the risk of incident heart failure in adults of European and African ancestry: a prospective meta-analysis from the cohorts for heart and aging research in genomic epidemiology (CHARGE) consortium. Circ. Cardiovasc. Genet. 3 (3), 256–266. https://doi.org/10.1161/CIRCGENETICS.109.895763. Epub 2010 May 5 PMID: 20445134.

Stevenson, J.G., Sayegh, R., Pedicino, N., Pellitier, N.A., Wheeler, T., Bechard, M.E., Huh, W.J., Coffey, R.J., Zemper, A.E. Lrig3 restricts the size of the colon stem cell compartment. Preprint at bioRxiv 2022.03.08.483523; doi: 10.1101/2022.03.08.483523.

Suzuki, Y., Sato, N., Tohyama, M., Wanaka, A., Takagi, T., 1996. cDNA cloning of a novel membrane glycoprotein that is expressed specifically in glial cells in the mouse brain. LIG-1, a protein with leucine-rich repeats and immunoglobulin-like domains. J. Biol. Chem. 271 (37), 22522–22527. https://doi.org/10.1074/jbc.271.37.22522. PMID: 8798419.

Thayer, T.E., Lino Cardenas, C.L., Martyn, T., Nicholson, C.J., Traeger, L., Wunderer, F., Slocum, C., Sigurslid, H., Shakartzi, H.R., O'Rourke, C., Shelton, G., Buswell, M.D., Barnes, H., Neitzel, L.R., Ledsky, C.D., Li, J.P., Burke, M.F., Farber-Eger, E., Perrien, D.S., Kumar, R., Corey, K.E., Wells, Q.S., Bloch, K.D., Hong, C.C., Bloch, D. B., Malhotra, R., 2020. The role of bone morphogenetic protein signaling in non-alcoholic fatty liver disease. Sci. Rep. 10 (1), 9831. https://doi.org/10.1038/s41598-020-66770-8. PMID: 32561790.

Thoolen, B., Maronpot, R.R., Harada, T., Nyska, A., Rousseaux, C., Nolte, T., Malarkey, D. E., Kaufmann, W., Küttler, K., Deschl, U., Nakae, D., Gregson, R., Vinlove, M.P., Brix, A.E., Singh, B., Belpoggi, F., Ward, J.M., 2010. Proliferative and nonproliferative lesions of the rat and mouse hepatobiliary system. Toxicol. Pathol. 38 (7 Suppl), 5S–81S. https://doi.org/10.1177/0192623310386499. PMID: 21191096 Review.

Vacca, M., Leslie, J., Virtue, S., Lam, B.Y.H., Govaere, O., Tiniakos, D., Snow, S., Davies, S., Petkevicius, K., Tong, Z., Peirce, V., Nielsen, M.J., Ament, Z., Li, W., Kostrzewski, T., Leeming, D.J., Ratziu, V., Allison, M.E.D., Anstee, Q.M., Griffin, J.L., Oakley, F., Vidal-Puig, A., 2020. Bone morphogenetic protein 8B promotes the progression of non-alcoholic steatohepatitis. Nat Metab. 2 (6), 514–531. https://doi.org/10.1038/s42255-020-0214-9. Epub 2020 PMID: 32694734.

Verdaguer, J.M., Trinidad, A., González-García, J.A., García-Berrocal, J.R., Ramírez-Camacho, R., 2006. Spontaneous otitis media in Wistar rats: an overlooked pathology in otological research. Lab Anim (NY). 35 (10), 40–44. https://doi.org/10.1038/laban1106-40. PMID: 17077834.

Wang, Y., Poulin, E.J., Coffey, R.J., 2013. LRIG1 is a triple threat: ERBB negative regulator, intestinal stem cell marker and tumour suppressor. Br. J. Cancer 108 (9), 1765–1770.

Wong, V.W., Stange, D.E., Page, M.E., Buczacki, S., Wabik, A., Itami, S., van de Wetering, M., Poulsom, R., Wright, N.A., Trotter, M.W., Watt, F.M., Winton, D.J., Clevers, H., Jensen, K.B., 2012. Lrig1 controls intestinal stem-cell homeostasis by negative regulation of ErbB signalling. Nat. Cell Biol. 14 (4), 401–408.

Xu, L., Bickhart, D.M., Cole, J.B., Schroeder, S.G., Song, J., Tassell, C.P., Sonstegard, T.S., Liu, G.E., 2015. Genomic signatures reveal new evidences for selection of important traits in domestic cattle. Mol. Biol. Evol. 32 (3), 711–725. https://doi.org/10.1093/molbev/msu333. Epub 2014 Nov 26 PMID: 25431480.

Zhou, J., Chang, Y., Li, J., Bao, H., Wu, C., 2023. Integrating whole-genome resequencing and RNA sequencing data reveals selective sweeps and differentially expressed genes related to nervous system changes in Luxi Gamecocks. Genes (Basel) 14 (3), 584. https://doi.org/10.3390/genes14030584. PMID: 36980855.